Hydrodynamics of Diamond-Shaped Gradient Nanopillar Arrays for Effective DNA Translocation into Nanochannels

(Supplementary information)

Chao Wang [1†‡], Robert L. Bruce [†], Elizabeth A. Duch [†], Jyotica V. Patel [†], Joshua T. Smith [†], Yann Astier [†], Benjamin H. Wunsch [†], Siddharth Meshram [†], Armand Galan [†], Chris Scerbo [†], Michael A. Pereira [†], Deqiang Wang [†], Evan G. Colgan [†], Qinghuang Lin [†], and Gustavo Stolovitzky *[†]

[†] IBM T.J. Watson Research Center, Yorktown Heights, NY 10598, USA

[‡] School of Electrical, Computer and Energy Engineering, Arizona State University, Tempe, AZ 85287, USA

1. Device fabrication and experiment

1.1 Oxidation to reduce nanofluidic channel dimensions

The dimensional reduction effect by oxidation is clearly seen by comparing the wafers before oxidation and afterwards (Figures S1) at the nanochannel interface. The oxidation reduced the width of originally 185 nm Si channels (Figure S1 a) to 100 nm (Figure S1 b) and that of 115 nm channels (Figure S1 c) to just ~30 nm (Figure S1 d). Additionally, the oxidation also shrunk the nano-pillar gap size from ~235 nm to ~150 nm.

In our fabrication, the patterned Si (100) substrate was thermally grown with SiO_2 in a tube furnace using a 900°C wet oxidation process to further reduce the channel dimension. Using such a high-temperature process, the oxide growth rate is very stable and uniform over the whole wafer. Since the exposed Si nanochannel surfaces are (100) on both the channel bottom and the sidewalls, the oxide thickness is uniform in all directions. Although the corners of Si rectangular channels have effectively high-index Si surfaces during growth and thus slightly slower oxide growth rate, they have only a minor impact on the DNA flow. Besides, since the growth

[1] Address correspondence to wangch@asu.edu, gustavo@us.ibm.com.

temperature is still far from the Si melting temperature (1414 °C), the process maintains the nanochannel structure integrity and slightly improves line-edge roughness.

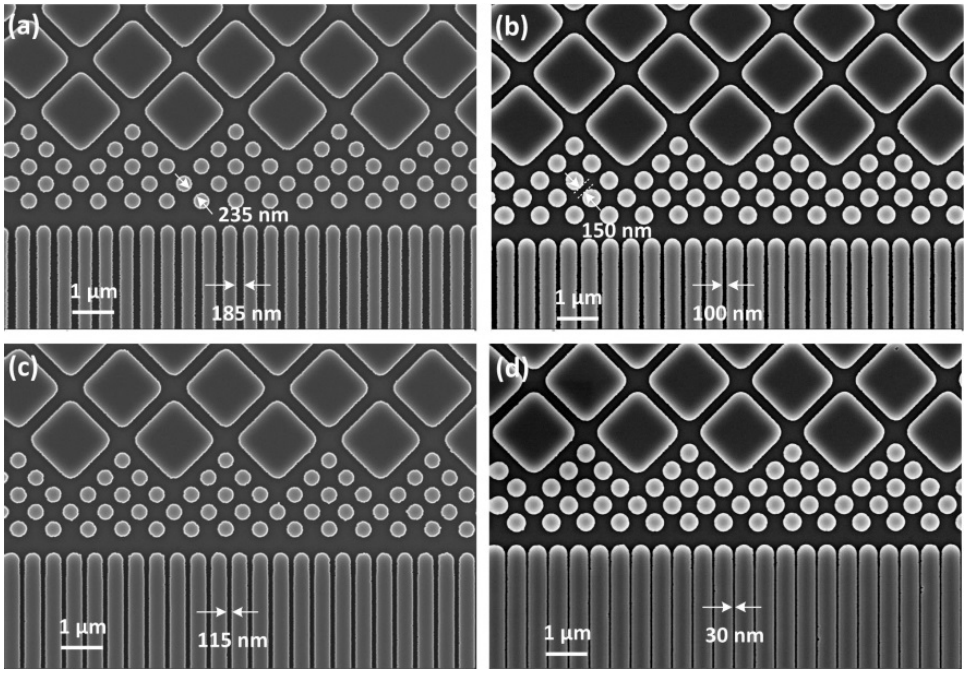

Figure S1. SEM images of nanofluidic feature dimensional control by oxidation. a-b, Nanofluidic channels with 100 nm final widths: (a) 235 nm gaps in pillar 4 region and 185 nm channels before oxidation; (b) 150 nm pillar gaps and 100 nm channels after 80 nm SiO_2 growth. c-d, Nanofluidic channels with 30 nm final widths: (c) 115 nm channels before oxidation; (d) 30 nm channels after oxidation.

1.2. Packaging of flow cells

The diced Si chip was bonded to a coverslip (Figure S2 a), with machined 1 mm access holes on the coverslip aligned to the fluidic microchannels on the chip (Figure S2 b). The bonded chip was aligned to the fluidic reservoirs on the customized fluidic jig (Figure S2 c), which has three components: a mounting base for leveling and positioning the chip, a flow chamber with fluidic access ports for sample handling, and a pump connector to provide a vacuum driving force. The flow chamber was designed with a rectangular opening in its center to accommodate 100X oil-immersion objectives for fluorescently imaging the DNA in all the critical nanofluidic regions (Figure S2 d). The customized fluidic system (Figure S2 e) allows us to simultaneously image the DNA translocation and control the hydrodynamic or electrophoretic flow.

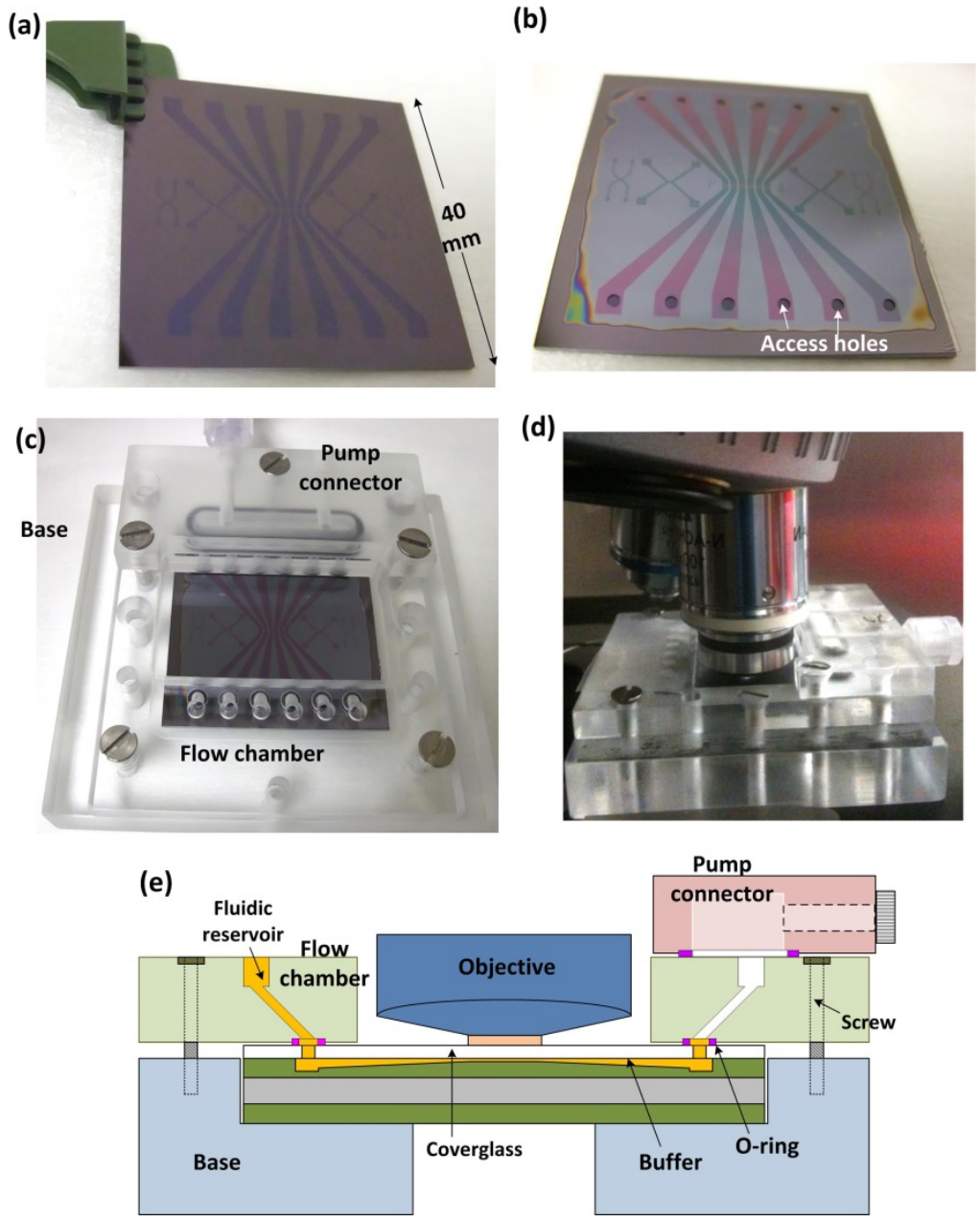

Figure S2. Packaging of fabricated nanofluidic chips. a-b, Optical images showing a chip: (a) after dicing and cleaning; (b) sealed by 170 µm thick Borofloat coverslips with drilled fluidic ports aligned to microchannel reservoirs. c-e, Sample handling and fluorescence imaging of DNA nanofluidic chips using a customized fluidic jig: (c) an optical image showing mounting a sealed fluidic chip on a jig; (d) an optical image showing the fluorescence imaging capability on an upright microscope; (e) The schematic of the fluidic system.

1.3. Estimation of λ-DNA translocation frequency

In our experiment, we intermittently recorded 350 DNA translocation events in 17 videos with recording duration of ~300 seconds. Given the imaged area of ~82 μm by ~82 μm and a nanochannel region of 700 μm, we estimate the DNA translocation rate in each second over the 700 μm wide nanochannel region (1400 channels) is roughly $f = \frac{350}{300} \times \frac{700}{82} = 10$. Assuming this rate, we estimate that ~18,000 DNA translocation events should have occurred during the 30 min experiment time.

2. Dependence of DNA speed parameters on nanostructure geometry

In a conserved nanofluidic system, the fluidic volume flowing across any region at a given time should be identical, no matter what the nano-confinement dimension is. Therefore, the flow speed changes as the allowed cross-sectional area changes in different patterned regions. To quantify the flow speed difference, we define a parameter, normalized fluidic cross-sectional factor F, as the percentage of cross-sectional area allowed for fluidic flow. For example, for a nanochannel with width W, depth d and period P (Figure S3 a), the ratio is simply

$$F = \frac{W \cdot d}{P \cdot d} = \frac{W}{P} \qquad \text{(equation S1)}$$

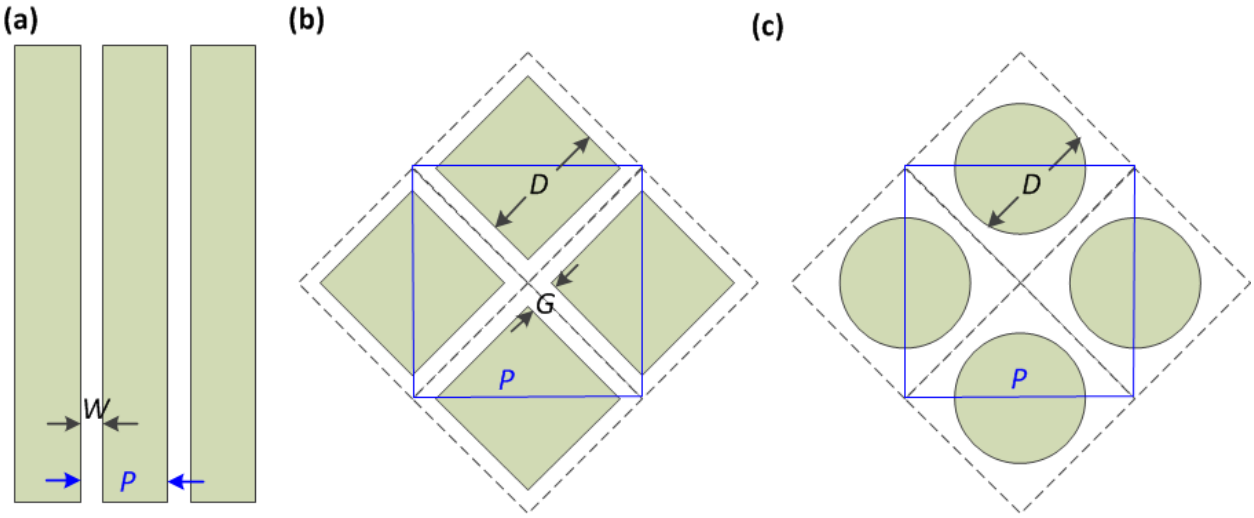

Figure S3. The schematics for calculating normalized fluidic cross-sectional area A_F. (a) A nanochannel with width W, depth d and period P; (b) Diamond pillar arrays with diamond side length D, gap size G, and period P; (c) Round pillar arrays with pillar diameter D and period P.

For diamond pillar arrays 1, 2, and 3 (Figure S3 b) with diamond side length D, gap size G and period P, we have:

$$F = \frac{P^2 - 2D^2}{P^2} \quad \text{(equation S2)}$$

$$P = \sqrt{2} \cdot (D + G) \quad \text{(equation S3)}$$

And for round pillar array 4 (Figure S3 c), we have

$$F = \frac{P^2 - 2\pi(\frac{D}{2})^2}{P^2} \quad \text{(equation S4)}$$

The cross-sectional area allowed for flow is thus

$$A_F = F \cdot (W_F \cdot d) \quad \text{(equation S5)}$$

where $W_F = 700\,\mu m$ is the nanofluidic feature coverage from pattern design and $d = 60\,nm$ is the etched fluidic depth. In our design, all nanochannel and nanopillar features have the same W_F and d. Because of the conservation of fluidic volume transported through any regions given a time interval τ at speed v, i.e.

$$V = A_F \cdot L = (FW_F d) \cdot (v\tau) \equiv Const. \quad \text{(equation S6)}$$

the product of Fv should be a constant across the nanofluidic pillars and channels. Therefore, the flow velocity changes accordingly, dependent on the nanostructure geometries, as calculated in Table S1 and plotted in Figure S4.

Table S1. Calculation of flow speed dependence on critical dimensions of nano-pillars and nanochannels in two devices. Here v/v_c is the flow speed ratio compared to that in nanochannels.

		W (nm)		P (nm)	d (nm)	F	v/v_c
Device 1 (shown in Figure 2)	channel	100		500	180	0.2	1
		G (nm)	D (nm)	P (nm)	d (nm)	F	v/v_c
	pillar 1	1200	5900	10000	180	0.30	0.66
	pillar 2	550	3000	5000	180	0.28	0.71
	pillar 3	240	1550	2500	180	0.23	0.87
	pillar 4	150	450	830	180	0.88	0.37
		W (nm)		P (nm)	d (nm)	F	v/v_c
Device 2 (shown in Figure 5 and Figure S5)	channel	160		1000	220	0.16	1
		G (nm)	D (nm)	P (nm)	d (nm)	F	v/v_c
	pillar 1	1430	5630	10000	220	0.37	0.44
	pillar 2	750	2820	5000	220	0.37	0.44
	pillar 3	380	1400	2500	220	0.37	0.43
	pillar 4	370	250	830	220	0.86	0.19

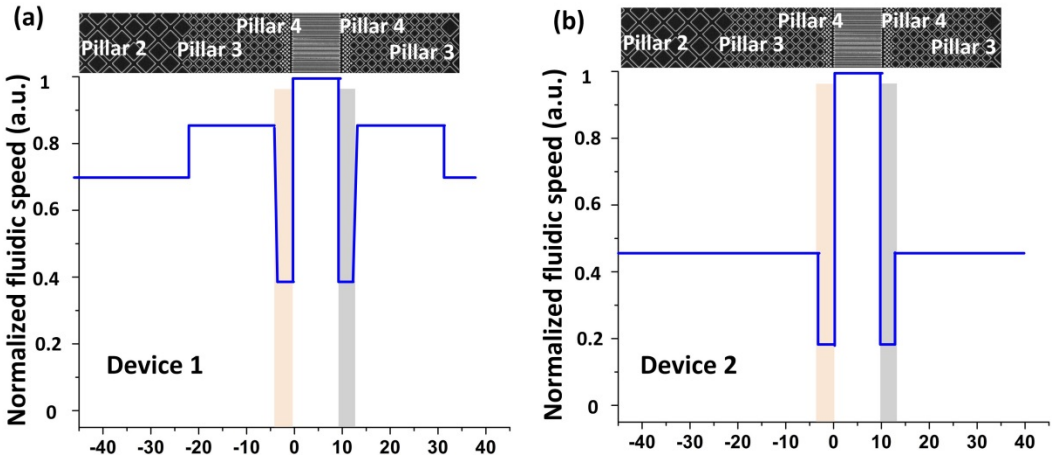

Figure S4. Calculated fluidic flow speed normalized to that in the channel for the two devices in Table S1: (a) device 1; (b) device 2.

3. DNA electrophoresis in 10 µm long nanochannels

We also used electrophoresis to drive the λ-DNA to translocate through the integrated nanopillars and nanochannels, and tuned the overall DNA speed in the imaged region from ~300 µm/sec to ~900 µm/sec by adjusting the external bias from 20 V to 50 V (Figure S5). We estimate about 18 % of externally applied voltage would drop onto the integrated nanofluidic region. Accordingly, the DNA mobility was determined as $(4.1 \pm 0.5) \times 10^{-4}\ cm^2/(V \cdot \text{sec})$.

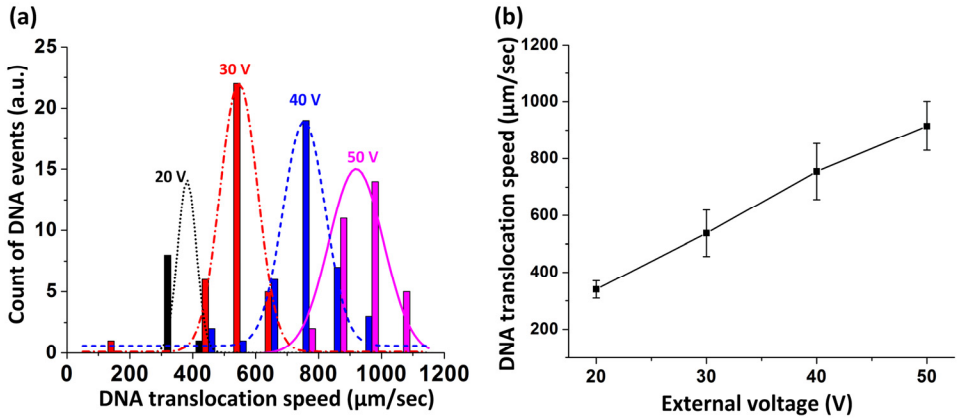

Figure S5. Electrophoresis driven λ-DNA translocation through nanopillars and nanochannels (100 nm wide and 10 µm long). (a) Statistics of DNA speeds at different external voltages, with the Gaussian fitting curve shown as black dot line, red dash-dot line, blue dash line, and magenta solid line for 20V, 30V, 40V, 50V external voltages, respectively. (b) The average DNA speeds at different voltages, showing a linear extrapolation and a uniform mobility.

We also noticed that DNA speed deviated more at a higher voltage (30-50V). This can be attributed to the complex DNA hydrodynamic behaviors inside the channels and pillars at higher voltages. Particularly, more abrupt speed change could result from interactions with the pillars: first, DNA straddled onto pillars at a higher speed, resulting in a sudden loss of momentum and a strong friction force from the pillars; second, the electric field applied on both ends of straddled DNA is higher, hence acting against releasing DNA from the pillars.

4. DNA translocation into a 50 µm long nanochannel device.

To study in detail the DNA translocation in longer channel, we fabricated a second nanofluidic device, incorporating 50 µm long, 220 nm deep, 160 nm wide, and 1 µm pitch nanochannels (Figure S6). The fabrication process is similar to that used for device 1, except that both the microchannel and integrated nanofluidic structures were etched into 1 µm oxide coated on Si substrate and no further Si oxidation was implemented. The SEM images of the structures are shown in Figure S6, with the nanochannel and nanopillar dimensions given in Table S1.

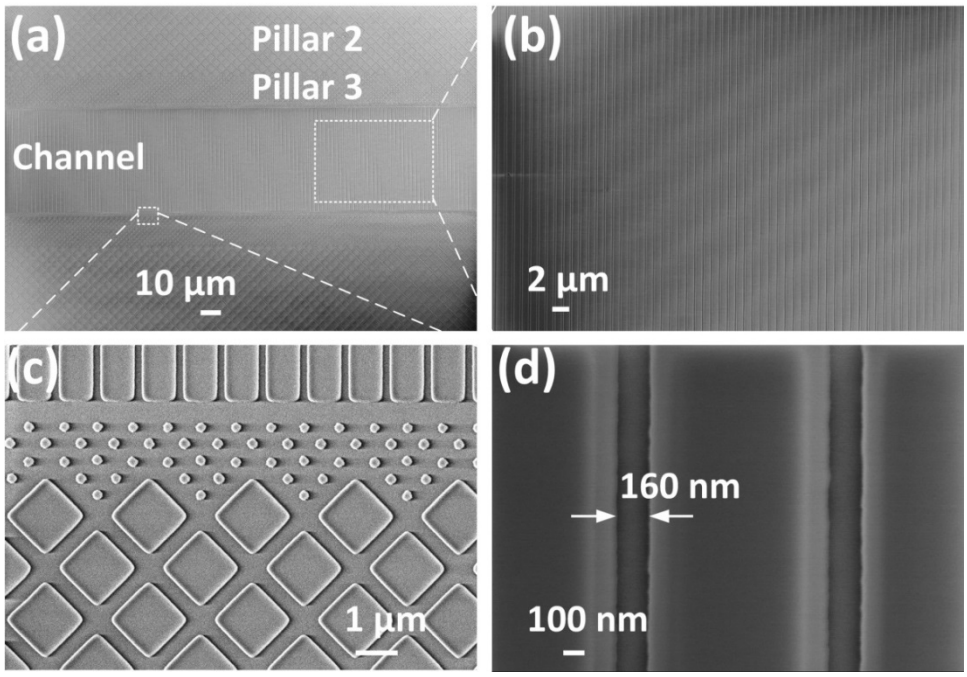

Figure S6. SEM images of an integrated nanofluidic chip with nanopillars and 50 µm long nanochannels. (a) Low-magnification image showing the structures of the nanofluidic chip. (b) An image showing about ~40 µm long portion of the nanochannel region with good uniformity. (c) The nanochannel entrance/exit vicinity with nanopillars. (d) High-magnification image showing ~160 nm wide nanochannels.

The complete DNA translocation event in the 50 μm long channel is revealed by the consecutive fluorescence images in Figure S7a, which supplement more information on the DNA hydrodynamic interactions with the nanochannel vicinities. The DNA head speeds and tail speeds collected from 30 DNA events were plotted in Figure S7b, showing the spatial dependence of the DNA translocation process.

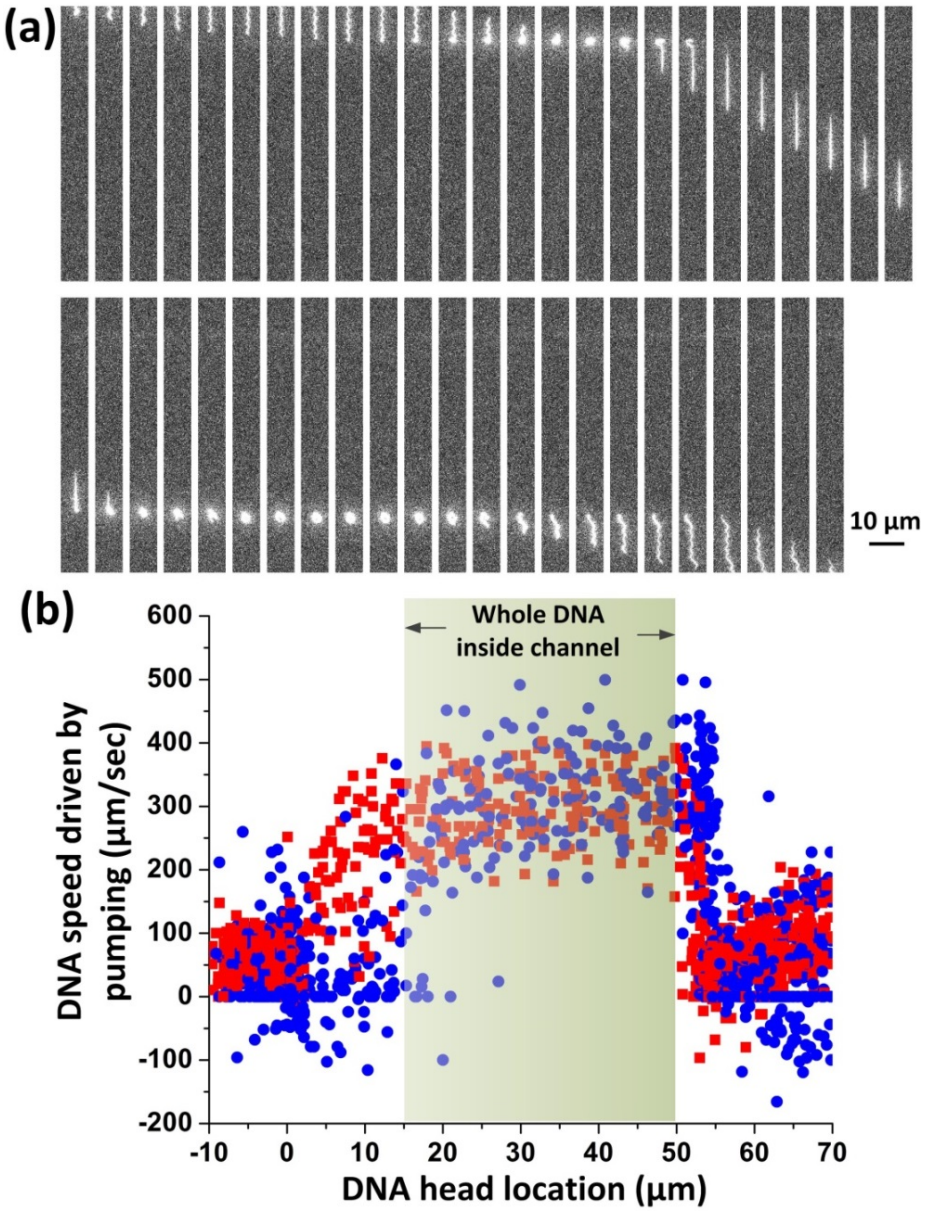

Figure S7. DNA translocation into 50 μm long nanochannels by pumping. (a) Consecutively recorded fluorescence images of DNA translocation under pumping. (b) Plot of DNA head speeds (red squares) and tail speeds (blue circles) during DNA translocation.

5. Stretching T4 DNA at low speed

The T4 molecules were driven hydrodynamically to flow at greatly reduced speed of ~20 μm/sec into a 5 μm long channel (Figure S8). Interestingly, the T4 DNA was able to straddle onto nanopillars and extend to 65.8 μm, or 90 % of its dye-labeled contour length (frame 214).

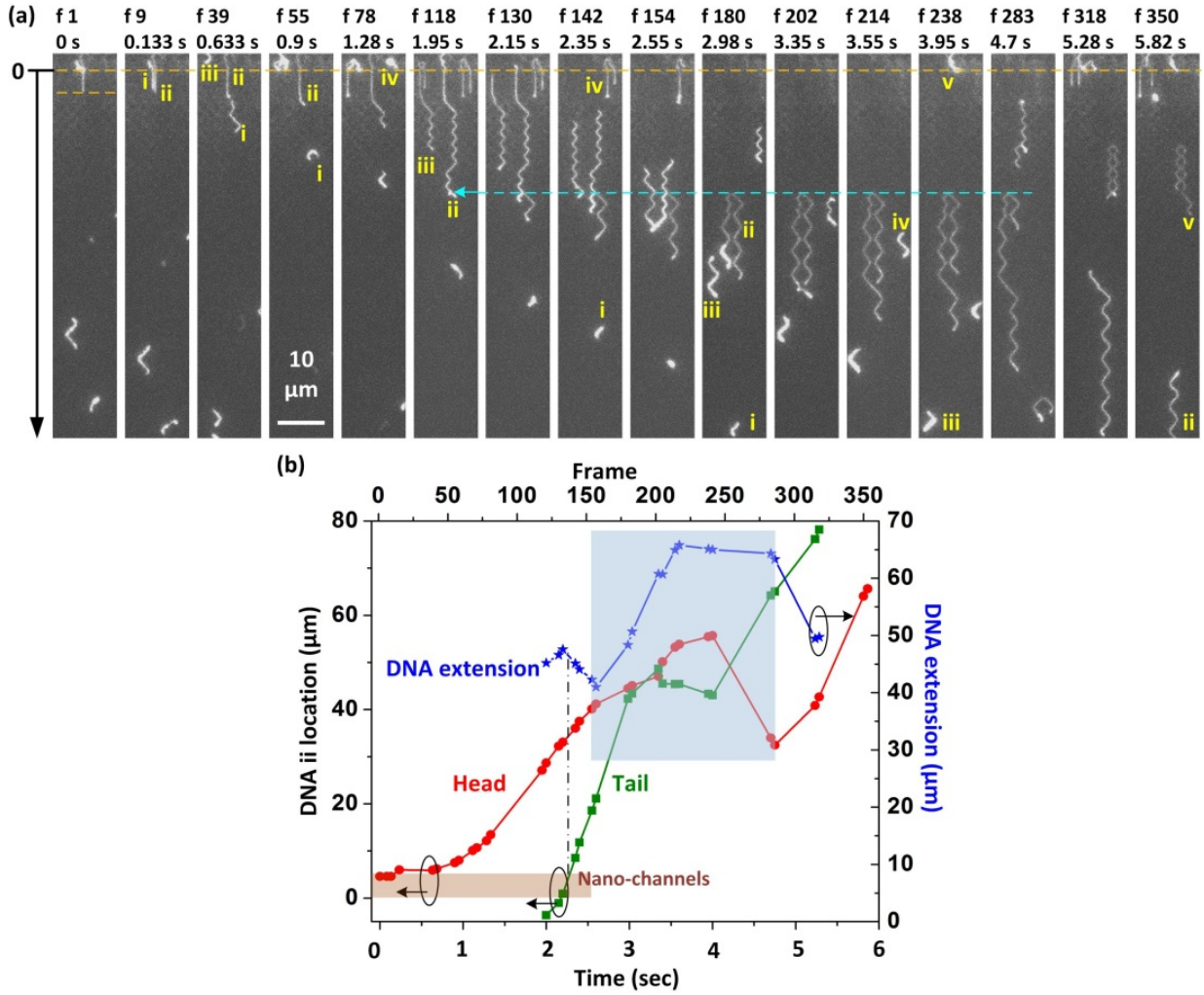

Figure S8. T4 DNA flow through nanofluidic chips at reduced flow speed. (a) Representative fluorescence images of DNA molecules. (b) The head/tail positions and extension of DNA ii molecule, with the shaded are indicating the straddling of DNA and the vertical dash-dot line indicating the exit of DNA tail from nanochannel.